Surface Science 622 (2014) 1–8

Contents lists available at ScienceDirect

Surface Science

journal homepage: www.elsevier.com/locate/susc

Adsorption of hydrazine on the perfect and defective copper (111) surface: A dispersion-corrected DFT study

Saeedeh S. Tafreshi, Alberto Roldan, Nelson Y. Dzade, Nora H. de Leeuw *

Department of Chemistry, University College London, 20 Gordon Street, London WC1H 0AJ, UK

ARTICLE INFO

Article history:
Received 15 October 2013
Accepted 22 November 2013
Available online 1 December 2013

Keywords:
DFT
Copper surface sites
Hydrazine adsorption
Dispersion correction

ABSTRACT

We have investigated the adsorption of hydrazine (N_2H_4) on perfect and defect-containing copper (111) surfaces by first-principles calculations. The long-range interactions are included in the geometry optimization through the application of the generalised gradient approximation with dispersion correction, DFT-D2 in the method of Grimme. We have studied three types of defects at the surfaces: monoatomic steps, Cu-adatoms and vacancies, where our calculations show that the adsorption energy increases as the coordination of the adsorption sites decreases. The ideal (111) is the most stable surface with the weakest adsorption of hydrazine, whilst the stepped (111) surface is the least stable and hence more reactive surface with the highest adsorption energy, where the hydrazine bridges across the step edge. We found that inclusion of the dispersion correction results in significant enhancement of molecule–substrate binding, thereby increasing the adsorption energy. This strong adsorption results in a bridging adsorption geometry for hydrazine, with a rotation around the N – N bond where the torsional angle changes from a gauche towards an eclipsed conformer to help the molecule to bridge through both nitrogen atoms, in agreement with experimental evidence. The core-level binding shifts for the N(1 s) states upon N_2H_4 adsorption have been calculated at DFT level to provide further insight into the N_2H_4 adsorption process on the copper surfaces.

1. Introduction

Copper nanoparticles have considerable industrial significance due to their catalytic and optical properties, high conductivity and durability, at a much lower cost than other metals such as silver and gold [1]. As variations in their size and shape change their properties, by controlling the morphology of nanoparticles, we could tune them with the specific properties required for particular applications. Generating specific nanoparticles with defined morphologies depends on several parameters such as bulk solvent type, temperature, pressure, synthesis devices and concentration of the reducing agents such as (N_2H_4) hydrazine [2–9]. For instance, reverse micelle-based synthesis has achieved much in the way of controlling the size and shape of copper nanoparticles [10], although the underlying processes are still not fully understood. Surface properties are an important factor in controlling the shape of nanoparticles, and surface free energies which determine the equilibrium shape of nano-crystals, play an important role in crystal growth phenomena [11].

Hydrazine has applications in different technologies e.g. in proton exchange membranes (PEM), Direct Hydrazine Fuel Cells (DHFC), room-temperature hydrazine/air direct-liquid fuel cells (DLFC) based on the use of nanostructure copper electrodes, gas generation and micro rockets for artificial satellites [12–14]. Therefore, to understand the underlying processes occurring during nanoparticle formation or at the electrodes of the fuel cell, we need to focus on the interactions between N_2H_4 and the metal surfaces. Computational techniques based on the Density Functional Theory (DFT) have become an important tool to unravel the interactions between adsorbates and metallic surfaces and they are used here to improve our understanding of copper nanoparticle production methods by investigating the processes occurring at the molecular level.

Computational studies have often focused on the ideal surfaces, whereas real surfaces are never perfect and chemical processes often occur at defective sites. In this paper, we have carried out a comprehensive computational study based on DFT to obtain an atomistic understanding of the adsorption of N_2H_4, not only at the perfect (111) copper surfaces, but also at three defective Cu surfaces; containing vacancies, Cu-adatoms and surface steps, where the (111) terraces are offset by one atomic layer from plane to plane. Daff et al. [15,16] have previously investigated aspects of the copper–hydrazine system, but this earlier work did not include a correction for the dispersion contribution, and a comparison with the dispersion corrected calculations is therefore deemed valuable, since the standard DFT calculations are not capable of describing the long-range interactions properly [17,18]. In this study, we have applied the DFT-D2 method by Grimme [19,20], which is a recent approach to include dispersive interactions, to characterize the interaction of hydrazine with the Cu(111) surfaces.

* Corresponding author. Tel.: +44 2076791015; fax: +44 2076797463.
E-mail address: n.h.deleeuw@ucl.ac.uk (N.H. de Leeuw).

0039-6028/$ – see front matter © 2013 Published by Elsevier B.V.
http://dx.doi.org/10.1016/j.susc.2013.11.013

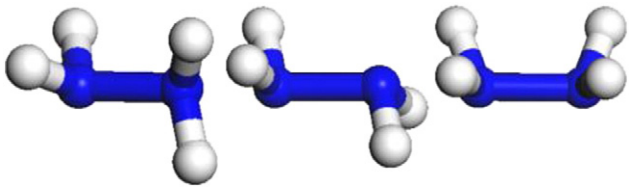

Fig. 1. Representation of the N_2H_4 conformations, from left to right: gauche, trans and eclipsed.

Table 1
Formation energies of Cu-adatom and vacancy on Cu(111).

Adatom-surface site	This work (eV)	Other works (eV)
fcc hollow	0.83	0.97 [37]
hcp hollow	0.85	
Bridge	1.01	
Top	1.19	
Vacancy	0.82	0.72 [37]

2. Computational methods

We have employed the Vienna ab-initio simulation package (VASP) [21,22] to perform DFT calculations [21–24]. We have used the projector augmented wave (PAW) and generalized gradient approximation (GGA) potentials [25,26], with the Perdew–Burke–Ernzerhof (PBE) exchange-correlation functional [27], to carry out our total energy calculations and perform geometry optimisations by minimizing the forces and stress tensor on the copper surfaces. To improve the description of the long-range interaction, we have employed the DFT-D2 [20] method of Grimme as implemented in VASP. In this approach the total energy is calculated as a function of the dispersion coefficient for each atom pair, a global scaling factor that depends only on the exchange-correlation functional used, which is 0.75 for the PBE functional, and a damping function to avoid near singularities for small distances. Although the Grimme dispersion coefficients were fitted against molecular properties rather than bulk materials, they are suitable in this work as we primarily compare trends in hydrazine–copper interactions between different surface geometries and adsorption configurations. As the dispersion interaction between the Cu atoms has the same energy contribution in each simulation, only the dispersion effect on the Cu–N_2H_4 and N_2H_4–N_2H_4 interactions varies significantly, which is adequately described by the Grimme coefficients.

The cut-off energy for the expansion of the plane-wave basis sets was set at 600 eV, which gave bulk energies converged to within 0.001 eV/atom. The integration of the Brillouin zone was done using a Monkhorst–Pack [28] 11 × 11 × 11 k-point grid in the bulk simulation. A lattice parameter of 3.571 Å was obtained from the bulk optimisation for the face-centred cubic (fcc) unit cell with an error of ~1.2% compared to the experimental value of 3.614 Å [29]. Subsequently, the ideal (111) surface and the planes with Cu adatoms and vacancies were modelled by a 3 × 3 × 1 k-point grid and each full unit cell has been grown into a 3 × 3 supercell (6 × 6 supercell from primitive supercell), which corresponds to a N_2H_4 coverage (θ_{N_2H4}) of 0.03 ML where ML is defined as the number of molecules divided by the number of Cu atoms on the surface. The adsorbate molecule and the three top-most surface layers were allowed to relax during structural optimisation, whilst the rest of the atoms in the slab were fixed at their bulk-optimised lattice positions. For the stepped Cu(111) surface, we have used a 5-layer 3 × 2 supercell giving a θ_{N_2H4} of 0.04 ML, relaxing the four uppermost layers and keeping one layer frozen, using a 3 × 5 × 1 k-point grid. This set-up, where one side of the slab is kept fixed, ensures the explicit geometry optimisation of a realistic number of surface layers, whilst still retaining a reasonably sized slab which made it feasible to investigate a large number of initial adsorption geometries. A vacuum of at least 20 Å was included between the slabs to avoid perpendicular interactions. We have also employed the dipole correction to enhance energy convergence.

To characterize the surface stabilities of various Cu surfaces we have computed the surface energy (γ) which is a measure of the thermodynamic stability of a given surface; the smaller its value the more stable the surface. The unrelaxed surface energy (γ_u) is calculated as follows, Eq. (1):

$$\gamma_u = \frac{E_{slab,u} - nE_{bulk}}{2A} \quad (1)$$

where $E_{slab,u}$ is the energy of the unrelaxed slab, E_{bulk} is the energy of the primitive cell, n is the number of atoms in the slab (because in the primitive bulk cell there is only one) and A is the surface area of one side of the slab. We have calculated the relaxed surface energy (γ_r) using Eq. (2); where $E_{slab,r}$ is the energy of the relaxed slab with one side fixed in the optimised bulk geometry.

$$\gamma_r = \frac{E_{slab,r} - nE_{bulk}}{A} - \gamma_u \quad (2)$$

The three major conformations of hydrazine in the gas phase: gauche, trans and eclipsed, are shown in Fig. 1. The gauche conformer is the lowest-energy structure, with the trans and eclipsed conformations 0.13 and 0.36 eV higher in energy respectively. We have started our investigation by placing the different N_2H_4 conformers in a number

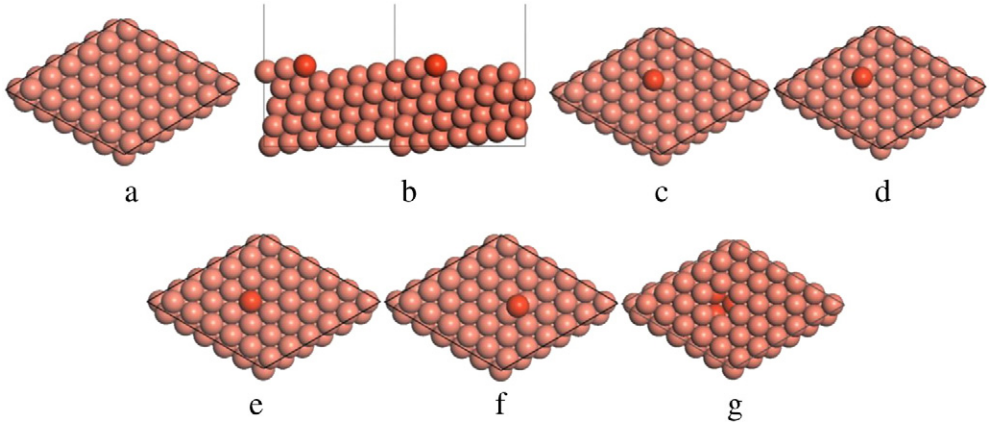

Fig. 2. The slab models used in the calculations of (a) perfect, (b) stepped, (c) fcc-adatom, (d) hcp-adatom, (e) top-adatom, (f) bridge-adatom and (g) surface vacancy (all structures are top views except for (b) which is a side view). Note that the copper adatoms, atoms in the second layer underneath the vacancy and low-coordinated atoms in stepped surfaces are shaded darker.

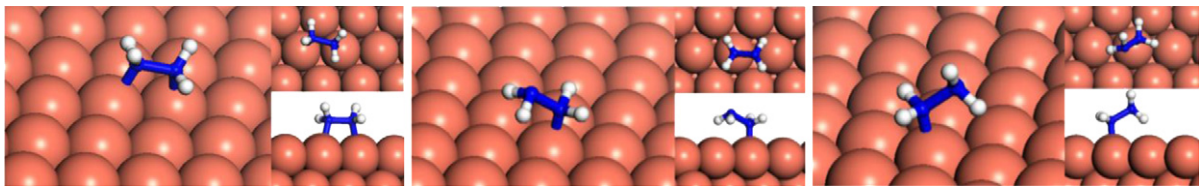

flat-a (-0.85 eV) flat-b (-0.85 eV) flat-c (-0.81 eV)

Fig. 3. The three lowest-energy configurations for adsorption of N_2H_4 on perfect Cu(111) surface. Adsorption energies are in parenthesis.

of initial configurations at a variety of positions on the perfect and defective Cu(111) surfaces in order to identify the lowest energy system. The adsorption energy (E_{ads}) was calculated as the difference between the total energy of the optimised substrate–adsorbate system ($E_{slab + mol}$) and the sum of the relaxed clean surface (E_{slab}) and isolated N_2H_4 in the gauche conformation (E_{mol}), Eq. (3):

$$E_{ads} = E_{slab+mol} - (E_{slab} + E_{mol}). \quad (3)$$

3. Results and discussion

3.1. Surface properties

We have first created the perfect Cu(111) surface, which shows the close-packed plane of the fcc structure (Fig. 2a) and is the most stable copper surface [15]. The surface energy is calculated to be 1.97 J m^{-2} which is in agreement with previously reported DFT studies [30,31,11] and experiments [32,33]. The surface Cu atoms are located in a hexagonal lattice with a separation of 2.52 Å between nearest neighbour atoms. However, as experimental surfaces and nanoparticles are not ideal, we have also created three defects on the (111) surface, namely: steps, adatoms and vacancies. The stepped (111) surface has been studied to investigate the presence of an extended edge of low-coordinated surface atoms. Each unit cell in the stepped slab (shown in Fig. 2b) was offset by one atomic layer with respect to the next cell, with six rows of copper atoms between each step [34–36].

As a point defect, we have investigated an adatom in a 3×3 supercell with one Cu atom added on one side of the slab, giving an ~3% coverage of Cu adatoms. The stacking of the planes of Cu atoms in the (111) direction is abc, where the Cu atoms in the fourth layer are directly underneath those in the first layer. Therefore, there are two types of hollow sites on the (111) terrace for the adatom to be located, each threefold coordinated by three close-packed Cu atoms in the surface. One site is directly above a Cu atom of the third sublayer – the face-centred-cubic (fcc) site (Fig. 2c) – and the other hollow site is directly on top of a Cu atom in the second sublayer – the hexagonal-close-packed (hcp) site (Fig. 2d). We have also studied two other sites for the adatom, i.e., exactly on top of one of the Cu surface atoms (Fig. 2e) and in a bridge site, between an fcc and hcp site (Fig. 2f). During the relaxation of the latter two, the added copper atom always moved towards either the fcc or hcp hollow sites and we therefore fixed the copper adatom in its lateral directions to remain in the top and bridge positions, whilst allowing it to move freely perpendicular to the surface. These calculations enable us to obtain energies for these unstable adatom positions providing information, for instance, on pathways for adatom diffusion across the Cu surface.

The adatom formation energies are calculated as the energy to take an atom from its bulk and place it on the surface. As shown by the formation energies in Table 1, the fcc and hcp sites are the preferred locations for the added copper atoms, with the fcc the most favourable site. These energies are related to the surface energies which follow the same trend in the order fcc ≈ hcp > bridge > top. The fcc-adatom is the lowest in surface energy, thus, we have studied the adsorption of hydrazine on the fcc-adatom Cu(111) surface, which for the purposes of interacting with the adsorbate is almost identical to the hcp-adatom.

Finally, we have studied a surface vacancy in the 3×3 supercell of the Cu(111), where one of the thirty six atoms in the top layer has been removed from the slab leading to an ~3% concentration of vacancies (Fig. 2g). Our calculated values for single adatom and vacancy formation energies are slightly different from the work by Karimi et al. [37] where they used embedded-atom method and a molecular static simulation.

As expected, the presence of a low-coordinated site affects the surface stability and therefore creating defects has a destabilizing effect on the surface. However the surface energies of the defective and perfect surfaces are close enough that we may expect all these surface defects to occur under experimental conditions. If we consider the fcc-adatom Cu(111) as the most stable adatom surface with a surface energy of 2.04 J m^{-2}, the vacancy surface with $\gamma = 2.04$ J m^{-2} and the stepped surface with $\gamma = 2.10$ J m^{-2} we see that the average of these calculated surface energies and that of the perfect surface at $\gamma = 1.97$ J m^{-2} is 2.04 J m^{-2}, which is very close to the experimental surface energy of 2.02 J m^{-2} [32,33], especially as this is only a rough approximation of the effect of defect concentration on the average surface stability.

Table 2
Geometries and adsorption energies (E_{ads}) of relaxed N_2H_4 adsorbed structures on the ideal Cu(111) surface. The angle between the N – N bond and the surface plane is Θ, the N–N bond length in gas phase is 1.44 Å. Long-range interaction energy contributions to the adsorption energies are also reported.

Label	Geometry	E_{ads} (eV/N_2H_4)	E_{ads}^{vdw} (eV/N_2H_4)	N – Cu (Å)	N – Cu (Å)	N – N (Å)	Θ (°)
Flat-a	Bridge	−0.85	−0.61	2.16	2.17	1.46	0.3
Flat-b	Trans-atop	−0.85	−0.66	2.07	3.04	1.47	26.2
Flat-c	Gauche-atop	−0.81	−0.66	2.09	3.01	1.44	29.4

3.2. Adsorption of N_2H_4 at the perfect Cu(111)

We have investigated a number of initial adsorbed hydrazine configurations to ensure as far as possible that the lowest-energy configuration is obtained, rather than a local minimum. Fig. 3 shows the three lowest energy adsorption configurations obtained on the perfect Cu(111) with structural and energetic details listed in Table 2. The preferred adsorption structures on the perfect Cu(111) surface are for N_2H_4 in gauche or trans conformations, both releasing an E_{ads} of 0.85 eV/N_2H_4. Gauche N_2H_4 bonds through both nitrogen atoms to the surface with Cu – N distances of 2.16 and 2.17 Å with the molecule almost parallel to the surface (0.3°, Fig. 3-flat-a). The molecule rotates around the N – N bond, towards the eclipsed conformer with a torsional angle of 41.5° from the gauche conformer and the N – N bond distance is increased by 0.02 Å, whereas N_2H_4 in the trans conformation has one N atom in a position slightly displaced from the atop site on a Cu atom where the molecule is at an angle of 26.2° to the surface (Fig. 3-flat-b).

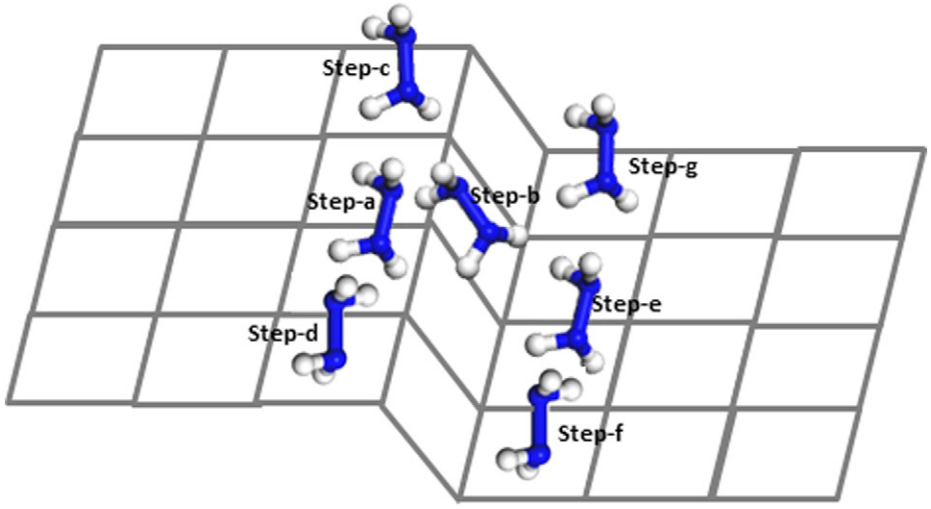

Fig. 4. Schematic illustration of initial adsorption configurations where N_2H_4 was placed at different sites on the step and terraces of the stepped Cu(111) surface.

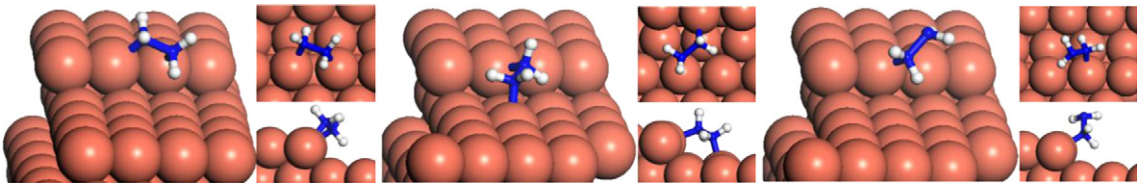

step-111a (-1.53 eV) step-111b (-1.34 eV) step-111c (-1.22 eV)

Fig. 5. The three lowest-energy configurations for adsorption of N_2H_4 on the stepped Cu(111) surface. Adsorption energies are given in parenthesis.

Only marginally less favourable is the situation where N_2H_4 is adsorbed in the gauche configuration releasing an energy of 0.81 eV/N_2H_4, with the N atom placed atop at a Cu–N distance of 2.09 Å and the molecule positioned at an angle of 29.4° to the surface (Fig. 3-flat-c).

Daff et al. [15], using pure DFT, obtained the lowest-energy configuration of hydrazine in the gauche conformation bound to only one Cu surface atom, releasing an adsorption energy of 0.42 eV/N_2H_4 [15], which is half of our calculated adsorption energy for the DFT-D calculation, where the N_2H_4 adsorbs to the surface through both N atoms. As the higher coverage used by Daff et al. may also have altered the adsorption structure, we have also calculated the hydrazine adsorption structures on the same size Cu(111) supercell to evaluate the impact of θ_{N_2H4} on the results. We found that in the smaller supercell identical to that of Daff et al., the molecule still adsorbs strongly to the surface, releasing even larger adsorption energy of 0.91 eV/N_2H_4, where the vdW contribution is −0.58 eV/N_2H_4. The pure DFT adsorption energy contribution is therefore only −0.33 eV/N_2H_4, i.e. differing by less than 0.1 eV/N_2H_4 from earlier reports [15], which is due to the different functional used (PBE in this work versus PW91 by Daff et al.). The van der Waals contribution is therefore significant and may even modify the nature of the interaction, as is for example found in the flat adsorption of pyridine on the Cu(110) surface, where the adsorption changed from physisorption (E_{ads} ~ −0.21 eV) to chemisorption (E_{ads} ~ −0.61 eV) [38]. A similar effect has been found in the self-assembly of uracil molecules on gold surfaces [39]. Our large surface simulation cell is also applied to the different defective surfaces, including adatoms, vacancy and stepped surfaces, thereby preventing the spurious interactions between any defect and its images.

Table 3
Geometries and adsorption energies (E_{ads}) of the relaxed N_2H_4 adsorbed structures on the stepped Cu(111) surface.

Label	Final geometry	E_{ads} (eV/N_2H_4)	N–Cu (Å)	N–Cu (Å)	N–N (Å)	Θ (°)
Step-a	Bridge-step	−1.53	2.09	2.12	1.46	15.2
Step-b	Bridge-step-terrace	−1.34	2.18	2.22	1.45	12.8
Step-c	Gauche-atop-step	−1.22	2.07	3.02	1.45	51.4
Step-d	Trans-atop-step	−1.16	2.04	3.02	1.48	28.4
Step-e	Bridge-terrace	−1.15	2.15	2.16	1.46	0.6
Step-f	Trans-atop-terrace	−1.09	2.09	3.07	1.47	27.8
Step-g	Gauche-atop-terrace	−1.06	2.12	3.06	1.44	27.6

3.3. Adsorption of N_2H_4 at the stepped Cu(111)

Next, we have investigated the adsorption of various conformations and configurations of the N_2H_4 molecule at different positions on the stepped Cu(111) surface. Fig. 4 shows a schematic illustration of the initial configurations where the molecule was placed either bridging across or atop Cu atoms on the step or in the vicinity on the surface. Fig. 5 shows the lowest-energy structures obtained after relaxation, whereas the adsorption energies and other structural parameters are summarized in Table 3. It can be seen that the adsorption configurations where N_2H_4 interacts with the low-coordinated step atoms lead to adsorption energies that are much larger than on the terrace.

The lowest energy structure (Fig. 5-step-a), with E_{ads} of −1.53 eV/N_2H_4 (E_{ads}^{vdW} = −0.44 eV/N_2H_4), was found by optimising the initial conformation where the molecule in its gauche conformation bridges two Cu atoms on the step edge with resulting Cu–N distances of 2.12 and 2.09 Å. The molecule rotates around its N–N bond and has a torsional angle of 59.0° relative to the eclipsed conformer. We have found that hydrazine can also bridge between two atoms, one on the step and another on the terrace with adsorption energy of −1.34 eV/N_2H_4

Table 4
Geometries and adsorption energies for the relaxed N_2H_4 adsorbed structures on the fcc-adatom Cu (111) surface. Long-range interaction energy contributions to the adsorption energies are also reported (bold numbers indicate a nitrogen atom is bound to the adatom).

Label	Geometry	E_{ads} (eV/N_2H_4)	E_{ads}^{vdW} (eV/N_2H_4)	E_{ads}, in [16] (eV/N_2H_4)	N – Cu (Å)	N – Cu (Å)	N – N (Å)	Θ (°)
fcc-a	Bridge-adatom-surface atom	−1.26	−0.65	−0.93	**2.08**	2.16	1.45	23.6
fcc-b	Gauche-atop-adatom	−1.18	−0.53	−1.09	**2.02**	2.92	1.46	0.5
fcc-c	Trans-atop-adatom	−1.18	−0.46	−1.09	**1.99**	2.91	1.48	10.9
fcc-d	Gauche-atop-surface atom	−0.82	−0.64	−0.52	2.09	3.01	1.44	29.3
fcc-e	Bridge-surface atoms	−0.81	−0.66	−0.49	2.16	2.17	2.17	0.3
fcc-f	Trans-atop-surface atom	−0.80	−0.69	−0.52	2.07	3.08	1.47	26.9

(Fig. 5-step-b). A local minimum energy structure is found when the gauche N_2H_4 is adsorbed through one N atom atop a step edge Cu atom at a distance of 2.07 Å, the molecule is inclined towards the terrace, releasing an E_{ads} of 1.22 eV/N_2H_4 (Fig. 5-step-c). In addition, we have studied configurations where the molecule is placed in the step vicinity. As shown in Table 3, the adsorption energies decrease as N_2H_4 adsorbs away from the step edge.

3.4. Adsorption of N_2H_4 at the adatoms and vacancies on the Cu(111)

The fcc site on the Cu(111) surface is the energetically preferred location for the adatom, and we have therefore investigated the adsorption of N_2H_4 near this adatom site in a number of different starting configurations. The description of the optimised geometries and the adsorption characteristics for the range of structures studied are given in Table 4, whereas Fig. 6 shows the lowest-energy adsorption configurations of the gauche and trans conformers of N_2H_4 on the fcc-adatom. The strongest adsorption, releasing an energy of 1.26 eV/N_2H_4, is obtained when the molecule bridges between the Cu-adatom and a surface copper atom at Cu – N distances of 2.08 and 2.16 Å respectively. The molecule is tilted to the surface at an angle of 9.4° and the N – N bond is rotated through an angle of 17.4° from gauche towards the eclipsed conformer (Fig. 6-fcc-a).

Two slightly less favourable locations for the molecule are atop the adatom bonded through one N atom and releasing 1.18 eV/N_2H_4 for both gauche and trans conformers (Fig. 6-fcc-b, c). We have also studied the structures where the gauche molecule is bound through both nitrogen atoms to the surface atoms next to the adatom (Fig. 6-fcc-e) or where a single N atom of N_2H_4 in gauche and trans conformations interacts with the surface far from the Cu-adatom (Fig. 6-fcc-d, f). These turn out to be local minima with adsorption energies in the range of −0.80 to −0.82 eV/N_2H_4, i.e. similar to the adsorption energy on the perfect surface indicating the local effect of the adatom. They are also significantly weaker than those for the molecule adsorbed at the adatom, either through bridging or atop modes. The defects thus provide stronger adsorption sites than the planar surface.

The adsorption energies on the fcc-adatom in this study are again larger than in previous work [16], where the most favourable adsorption geometry on the fcc-adatom Cu(111) surface had N_2H_4 bonded with one nitrogen on top of the adatom with an adsorption energy of −1.09 eV/N_2H_4, smaller than our E_{ads} for the same adsorbed configuration (−1.18 eV/N_2H_4) due to the inclusion of the long-range attractive

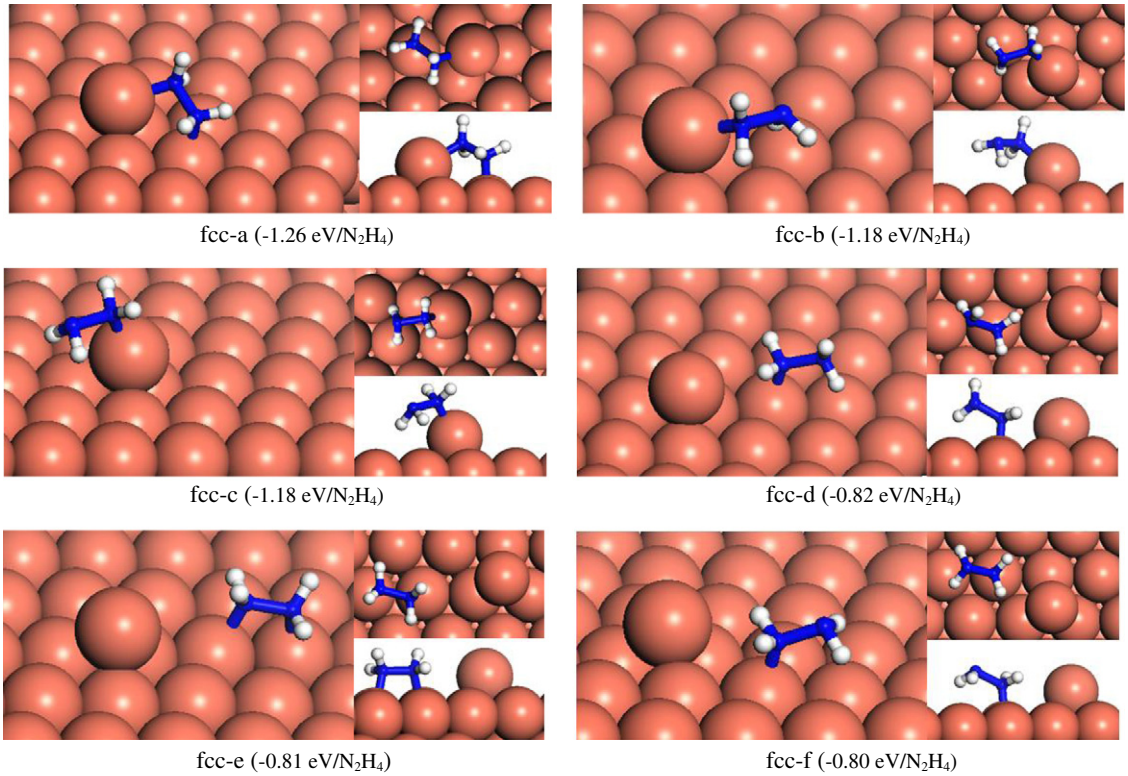

Fig. 6. The lowest-energy configurations of adsorption of N_2H_4 on fcc-adatom Cu(111) surface.

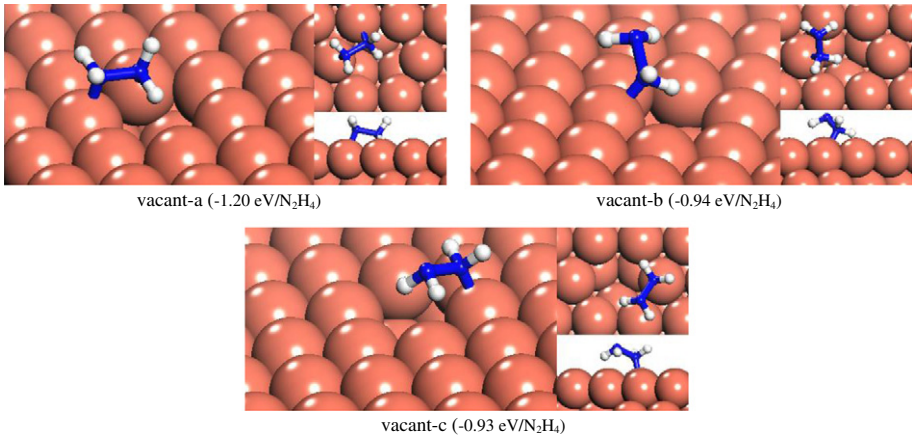

Fig. 7. The lowest-energy configurations for adsorption of N_2H_4 on vacant Cu(111) surface.

forces in this study. Furthermore, the dispersion correction also changed the preferred orientation of the molecule, which now prefers to interact through a bridging adsorption configuration rather than the atop geometry obtained by Daff et al. [16].

Finally, we have investigated the adsorption of N_2H_4 at the Cu vacancies on the (111) surface. The lowest-energy structures are schematically shown in Fig. 7, with geometric and energetic details summarized in Table 5. The strongest adsorption, releasing an energy of 1.20 eV/N_2H_4 (E_{ads}^{vdW} = 0.67 eV/N_2H_4), is found for a configuration where the molecule bridges between two copper atoms next to the vacancy at Cu–N distances of 2.09 and 2.13 Å and inclined to the surface by an angle of 12.5° (Fig. 7-vacant-a). In this adsorption structure, N_2H_4 rotates around the N–N bond with a torsional angle of 29.9° from gauche to eclipsed conformer.

Two local minima were found for the molecule adsorbed atop the atom next to the vacancy with different orientations of the gauche and trans conformers (Fig. 7-vacant-b, c) and adsorption energies of −0.94 and −0.93 eV/N_2H_4 respectively.

3.5. Electronic structure

In order to characterize the bond between N_2H_4 and the Cu surfaces, we have carried out an analysis of the electron density, where the charge density difference was obtained by subtracting from the charge density of the total adsorbate system, the sum of the charge densities of the molecule and the clean surface in the same geometry, Eq. (4):

$$\rho_{transfer} = \rho_{surf+mol} - (\rho_{surf} + \rho_{mol}). \quad (4)$$

Fig. 8 shows the induced charge density with an isovalue of ± 0.02 e/Å^3 on each surface upon N_2H_4 adsorption. It indicates the transferred charge densities which on the perfect Cu(111) originate primarily from the Cu atoms in the uppermost layer, whereas on the Cu step, adatom and partially vacant surfaces, the charge is transferred mainly from the unsaturated Cu atoms.

Table 5
Geometries and adsorption energies for the lowest-energy N_2H_4 adsorbed structures on the vacant Cu(111) surface.

Label	Geometry	E_{ads} (eV/N_2H_4)	N–Cu (Å)	N–Cu (Å)	N–N (Å)	Θ (°)
Vacant-a	Bridge	−1.20	2.09	2.13	1.45	12.5
Vacant-b	Gauche-atop	−0.94	2.07	2.97	1.47	32.9
Vacant-c	Trans-atop	−0.93	2.06	3.01	1.47	24.4

We have identified the amount of charge transferred between the molecule and the surfaces by using Bader analysis [40] for the preferred adsorption structures. As shown in Table 6, the calculated Bader charges suggest only a local charge redistribution within the N_2H_4/Cu systems as the resulting net charge transfer between the N_2H_4 and the Cu surfaces is very small (approximately 0.1 e$^-$). We found no trend between the amount of charge transferred and the calculated adsorption energies of N_2H_4 at the different Cu surfaces which indicates that the variation in strength of N_2H_4 binding may be an effect of the coordination of the interacting surface Cu atoms. In order to clarify this suggestion, we have analysed the adsorption energy per N atom in relation to the coordination number (CN) of the interacting Cu atoms. Within this approximation, the binding energy per N atom on the flat, stepped and vacancy-containing surface sites is obtained by halving their respective total adsorption energies since both interacting Cu atoms at these surfaces have the same CN. The adsorption energy per N atom at the adatom surface site is obtained by the difference between the total adsorption energy of hydrazine at the adatom surface and the adsorption energy per N on the flat surface. A plot of the adsorption binding energy per N atom as a function of the interacting Cu coordination numbers reveals a clear trend as shown in Fig. 9. It is evident from Fig. 9 that the adatom site (which has the lowest CN = 3) leads to the strongest binding and the flat surface (with the largest CN = 9) shows the weakest binding per N atom. These results are in good agreement with general surface observations, where surfaces with lower-coordinated surface sites are more reactive than those with almost saturated surface sites.

3.6. Calculation of core level binding energy shifts

Identification of adsorption structures assists our understanding of the mechanism of surface chemical reactions. X-ray photoelectron spectroscopy (XPS) is one of the most highly used spectroscopic techniques to identify the electronic and geometric structures of solid surfaces with adsorbed molecules. XPS can be compared directly with first-principles DFT calculations of the core-level binding energy shifts (CLS). In this section, we have calculated the CLS for the N(1 s) states upon N_2H_4 adsorption at DFT level to obtain better understanding of the N_2H_4 adsorption process on the copper surfaces.

The core-level binding energy is the energy required to remove a core electron from the atom of interest. At DFT level, the binding energy of core electrons (E_{CL}) is calculated as the energy difference between two separate calculations [41,42] as per Eq. (5). The first calculation is a standard DFT calculation in which the number of core electrons corresponds to the unexcited ground state ($E(n_c)$). In the second calculation one electron is removed from the core of one particular atom and added to the valence or conduction band ($E(n_c - 1)$). A total energy is then

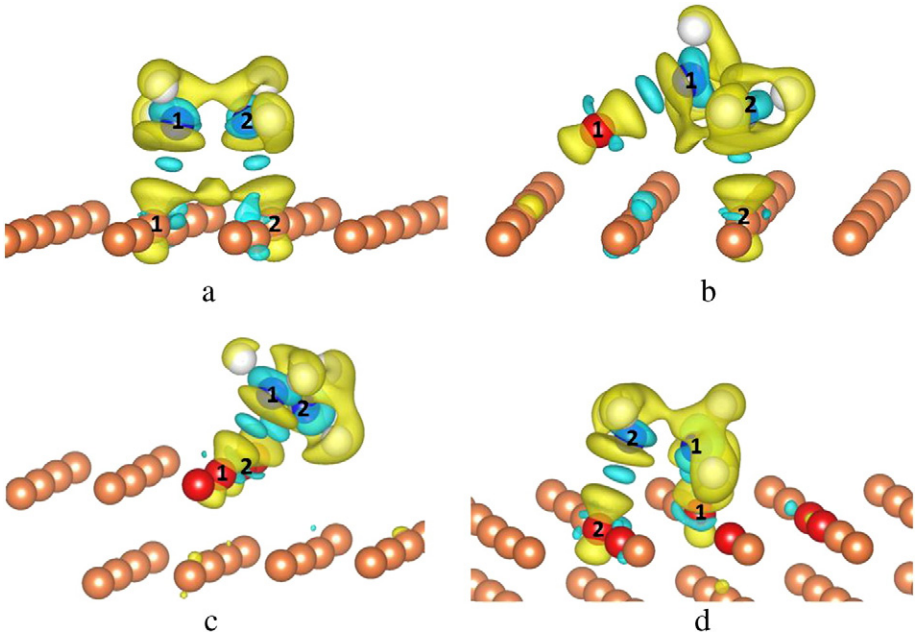

Fig. 8. Induced charge density presentation of the adsorption of N_2H_4 molecule on (a) perfect, (b) adatom, (c) step and (d) vacant Cu(111) surfaces by an isosurface of ±0.02 e/Å^3, where yellow and blue denote lost and gain of electron density. Low-coordinated atoms are shown in red.

obtained via minimization of electronic configuration in the presence of the core-hole.

$$E_{CL} = E(n_c - 1) - E(n_c) \quad (5)$$

Core-level binding energy shifts (E_{CLS}) are the changes in binding of specific core electrons (E_{CL}) of atoms of interest compared to reference atoms, which are typically located in a different environment, Eq. (6):

$$E_{CLS} = E_{CL} - E_{CL}^{ref}. \quad (6)$$

E_{CLS} can be compared to the experimentally determined value which is sensitive to the local environment. This calculation provides a unique way to gain detailed knowledge of adsorption sites and structures in a direct relation with experimental measurements. The chemical bonds are formed by orbital hybridization and often with charge transfer. In the case of molecular adsorption, the formation of a bond depends on the active site and their coordination leading to variations in E_{CL} for both adsorbates and substrates, which can be measured by X-ray photoelectron spectroscopy (XPS) and calculated computationally. To illustrate this, we present a CLS calculation for the most favourable adsorption structures on each Cu surface. In Table 7, we summarize the calculated CLS for N(1s) of both N atoms in N_2H_4 on the perfect, stepped, adatom and partially vacant Cu(111) surfaces. We obtained the biggest CLS for the geometries where the molecule bridges through both nitrogen atoms. As Fig. 10 shows, for weaker adsorption through one nitrogen, we found a shift to lower binding energies due to a major charge transfer from the Cu to that particular N in the N_2H_4 molecule. These results contrast with the experimental work by Littrell and Tatarchuk [43] where they have used in situ XPS to obtain a CLS of −6.1 eV for adsorption of N_2H_4 at 6×10^{-4} Torr and 295 K on an unspecific Cu surface. However, the CLS on the 1s-orbital of N derived from our calculations are in line with those measured and calculated for NO adsorption on the Pt(111) surface [44,45]. Those authors carried out a comprehensive investigation and revealed the sensitivity of the CLS with respect to the tilt angle and the distance between molecule and surface, indicating that the discrepancy between DFT and experiment may be due to the thermal vibration and rotation of adsorbed molecules. Experimental XPS measurements on well-defined surfaces at low temperatures would be comparable with our predicted results here, which would be helpful in confirming the CLS model.

Table 6
Atomic charges of adsorbed hydrazine and the interacting surface Cu atoms on different Cu surfaces. The atomic charges of gas-phase hydrazine are also reported.

System	N1 (e$^-$)	N2 (e$^-$)	H1 (e$^-$)	H2 (e$^-$)	H3 (e$^-$)	H4 (e$^-$)	Cu1 (e$^-$)	Cu2 (e$^-$)
Flat	−0.79	−0.75	0.41	0.41	0.45	0.41	0.12	0.12
Step	−0.77	−0.77	0.43	0.40	0.43	0.42	0.13	0.13
Adatom	−0.79	−0.75	0.42	0.39	0.43	0.43	0.18	0.14
Vacant	−0.79	−0.78	0.42	0.42	0.43	0.42	0.13	0.13
Gas-phase hydrazine	−0.73	−0.73	0.37	0.36	0.37	0.36		

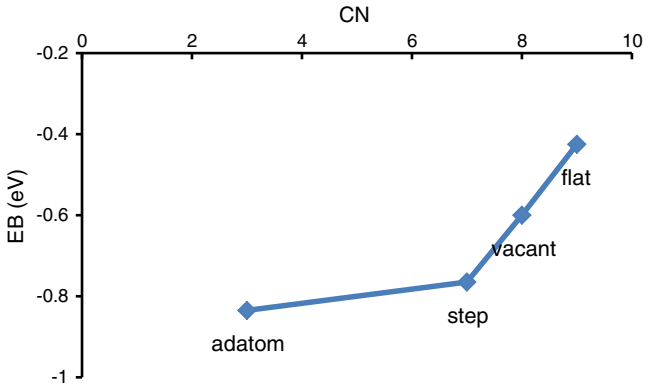

Fig. 9. Adsorption energies per nitrogen atom as a function of coordination number of interacting copper atoms for the lowest-energy adsorption structures on perfect and different defective Cu(111) surfaces.

Table 7
Core-level binding energy shifts (E_{CLS}) for both N(1s) for atoms of N_2H_4 on the strongest adsorption structures on the perfect, stepped, adatom and vacant Cu(111) surfaces.

Structure	Geometry	E_{ads} (eV)	E_{CLS} (eV)
Flat-111a	Bridge	−0.85	−0.45, −0.44
Flat-111c	Gauche-atop	−0.81	−1.48, −0.92
Step-111a	Bridge-step	−1.53	−0.32, 0.09
Step-111d	Gauche-atop-step	−1.22	−1.31, −0.90
Adatom-111a	Bridge-adatom-surface atom	−1.26	−0.47, −0.20
Adatom-111c	Gauche-atop-surface atom	−0.82	−1.50, −1.04
Vacant-111a	Bridge	−1.20	−0.55, −0.36
Vacant-111c	Trans-atop	−0.93	−1.73, −0.76

4. Conclusions

We have carried out a systematic study of N_2H_4 adsorption on ideal, stepped and point defect-containing (adatom, vacancy) Cu(111) surfaces using DFT level calculations with long-range interaction corrections. Our study has shown that the surface structure and the presence of defects have a significant effect on the adsorption of N_2H_4. Defect sites have lower coordination numbers than the perfect surface atoms making them more reactive. The planar Cu(111) surface offers the weakest adsorption to the molecule, whilst the highest adsorption energy is obtained on the least stable stepped (111) surface, where bridging of hydrazine on the low-coordinated atoms of the step edge is the preferred configuration. Our results, in comparison with previous work, indicate that the long-range interactions are important in determining the most favourable adsorption structures, which also lead to stronger bonds between Cu and N atoms inclining the molecule to the surface in bridging modes. This mode of adsorption is in agreement with that found by experiments [46,47] which suggest that a two-point attachment of the N–N of the N_2H_4 molecule occurs on Cu surfaces. This bridging structure was also proposed by Alberas et al. [48] for hydrazine on Pt(111), based on XPS and high resolution electron energy loss spectroscopy (HREELS) measurements, and by Grunze [49] on Fe(111), based on photoelectron spectroscopy experiments. In this study, we have also used larger simulation cells to obtain lower N_2H_4 coverages than previous work, which help to prevent interactions between the molecules in neighbouring cells and ensure that we calculate only the surface–adsorbate interactions of the isolated hydrazine molecule.

Future work will include the self-assembly process of hydrazine layers on the copper surfaces, determined by lateral intermolecular interactions between the molecules, as well as the dissociation through deprotonation of the hydrazine molecules. These studies will provide fundamental knowledge of the different processes of N_2H_4 on the metallic surface, which will improve our insight into the mechanisms occurring in Direct Hydrazine Fuel Cells and in room-temperature hydrazine/air direct-liquid fuel cells.

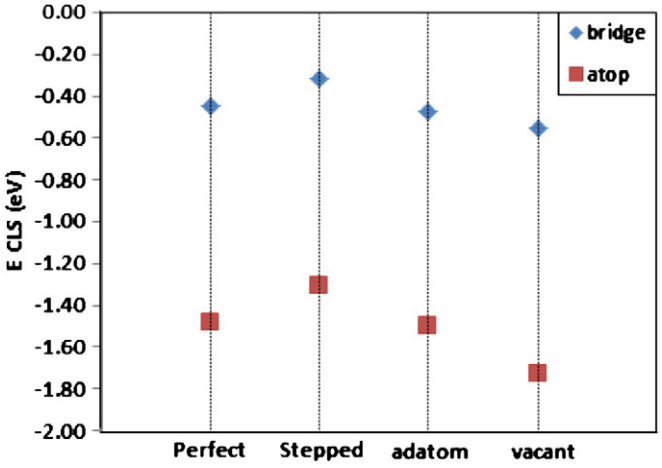

Fig. 10. Core-level binding energy shifts (E_{CLS}) for N(1s) of N_2H_4 in the strongest adsorption structures on the perfect, stepped, adatom and vacant Cu(111) surfaces.

Acknowledgements

S.S.T acknowledges University College London for an UCL Overseas Research Scholarship. NHdL acknowledges EPSRC (EP/G036675) for financial support. Dr. A. Roldan is grateful to the Ramsay Memorial Trust and University College London for the provision of a Ramsay Fellowship. Via our membership of the UK's HPC Materials Chemistry Consortium, which is funded by EPSRC (EP/F067496), this work made use of the facilities of HECToR, the UK's national high-performance computing service, which is provided by UoE HPCx Ltd at the University of Edinburgh, Cray Inc. and NAG Ltd, and funded by the Office of Science and Technology through EPSRC's High End Computing Programme, as well as the UCL Legion High Performance Computing facility (Legion@UCL), and associated support services, in the completion of this work.

References

[1] D.A. Jones, Principles and Prevention of Corrosion, Prentice Hall, Upper saddle River, NJ, 1996.
[2] A. Filankembo, S. Giorgio, I. Lisiecki, M.P. Pileni, J. Phys. Chem. B 107 (2003) 7492.
[3] C.L. Kitchens, M.C. McLeod, C.B. Roberts, J. Phys. Chem. B 107 (2003) 11331.
[4] I. Lisiecki, M.P. Pileni, J. Am. Chem. Soc. 115 (1993) 3887.
[5] M.P. Pileni, Langmuir 17 (2001) 7476.
[6] C. Salzemann, L. Lisiecki, J. Urban, M.P. Pileni, Langmuir 20 (2004) 11772.
[7] J. Tanori, M.P. Pileni, Adv. Mater. 7 (1995) 862.
[8] J. Tanori, M.P. Pileni, Langmuir 13 (1997) 639.
[9] Y.H. Wei, S. Chen, B. Kowalczyk, S. Huda, T.P. Gray, B.A. Grzybowski, J. Phys. Chem. C 114 (2010) 15612.
[10] I. Lisiecki, J. Phys. Chem. B 109 (2005) 12231.
[11] L. Vitos, A.V. Ruban, H.L. Skriver, J. Kollar, Surf. Sci. 411 (1998) 186.
[12] M.R. Andrew, W.J. Gressler, J.K. Johnson, R.T. Short, K.R. Williams, J. Appl. Electrochem. 2 (1972) 327.
[13] E. Granot, B. Filanovsky, I. Presman, I. Kuras, F. Patolsky, J. Power Sources 204 (2012) 116.
[14] K. Yamada, K. Asazawa, K. Yasuda, T. Ioroi, H. Tanaka, Y. Miyazaki, T. Kobayashi, J. Power Sources 115 (2003) 236.
[15] T.D. Daff, D. Costa, I. Lisiecki, N.H. de Leeuw, J. Phys. Chem. C 113 (2009) 15714.
[16] T.D. Daff, N.H. de Leeuw, J. Mater. Chem. 22 (2012) 23210.
[17] P. Hohenberg, W. Kohn, Phys. Rev. B 136 (1964) B864.
[18] W. Kohn, L.J. Sham, Phys. Rev. 140 (1965) 1133.
[19] S. Grimme, J. Comput. Chem. 25 (2004) 1463.
[20] S. Grimme, J. Comput. Chem. 27 (2006) 1787.
[21] G. Kresse, J. Furthmuller, Nato Sc S Ss Iii C S 6 (1996) 15.
[22] G. Kresse, J. Furthmuller, Phys. Rev. B 54 (1996) 11169.
[23] G. Kresse, J. Hafner, Phys. Rev. B 49 (1994) 14251.
[24] G. Kresse, J. Hafner, Phys. Rev. B 47 (1993) 558.
[25] P.E. Blochl, Phys. Rev. B 50 (1994) 17953.
[26] G. Kresse, D. Joubert, Phys. Rev. B 59 (1999) 1758.
[27] J.P. Perdew, K. Burke, M. Ernzerhof, Phys. Rev. Lett. 77 (1996) 3865.
[28] H.J. Monkhorst, J.D. Pack, Phys. Rev. B 13 (1976) 5188.
[29] M.E. Straumanis, L.S. Yu, Acta Crystallogr. A Cryst. 25 (1969) 676.
[30] I. Galanakis, N. Papanikolaou, P.H. Dederichs, Surf. Sci. 511 (2002) 1.
[31] H.L. Skriver, N.M. Rosengaard, Phys. Rev. B 46 (1992) 7157.
[32] H. Wawra, Z Metallkd. 66 (1975) 492.
[33] H. Wawra, Z Metallkd. 66 (1975) 395.
[34] N.H. de Leeuw, C.J. Nelson, J. Phys. Chem. B 107 (2003) 3528.
[35] N.H. de Leeuw, C.J. Nelson, C.R.A. Catlow, P. Sautet, W. Dong, Phys. Rev. B 69 (2004).
[36] N.H. de Leeuw, S.C. Parker, C.R.A. Catlow, G.D. Price, Am. Mineral. 85 (2000) 1143.
[37] M. Karimi, T. Tomkowski, G. Vidali, O. Biham, Phys. Rev. B 52 (1995) 5364.
[38] N. Atodiresei, V. Caciuc, J.H. Franke, S. Blugel, Phys. Rev. B 78 (2008).
[39] S. Irrera, A. Roldan, G. Portalone, N.H. De Leeuw, J. Phys. Chem. C 117 (2013) 3949.
[40] J. Tersoff, D.R. Hamann, Phys. Rev. B 31 (1985) 805.
[41] L. Kohler, G. Kresse, Phys. Rev. B 70 (2004).
[42] S. Lizzit, A. Baraldi, A. Groso, K. Reuter, M.V. Ganduglia-Pirovano, C. Stampl, M. Scheffler, M. Stichler, C. Keller, W. Wurth, D. Menzel, Phys. Rev. B 63 (2001).
[43] D.M. Littrell, B.J. Tatarchuk, J. Vac. Sci. Technol. A 4 (1986) 1608.
[44] Z.H. Zeng, J.L.F. Da Silva, H.Q. Deng, W.X. Li, Phys. Rev. B 79 (2009).
[45] Z.H. Zeng, X.F. Ma, W.C. Ding, W.X. Li, Sci. China Chem. 53 (2010) 402.
[46] Y.K. Alhaydari, J.M. Saleh, M.H. Matloob, J. Phys. Chem. 89 (1985) 3286.
[47] M.H. Matloob, M.W. Roberts, J. Chem. Soc. Faraday Trans. 1 (73) (1977) 1393.
[48] D.J. Alberas, J. Kiss, Z.M. Liu, J.M. White, Surf. Sci. 278 (1992) 51.
[49] M. Grunze, Surf. Sci. 81 (1979) 603.